

Article

Synthesis of TiC_x/Al Composites via In Situ Reaction between Al_xTi Melt and Dissolvable Solid Carbon

Lei Guo, Hao Sun and Zhancheng Guo *

State Key Laboratory of Advanced Metallurgy, University of Science and Technology Beijing, Xueyuan Road No. 30, Haidian District, Beijing 100083, China; leiguo@ustb.edu.cn (L.G.); m202121330@xs.ustb.edu.cn (H.S.)

* Correspondence: zcguo@ustb.edu.cn

Abstract: TiC_x/Al composites were successfully prepared in this study by dissolving graphite particles in Al-Ti melt based on the principle of a solid–liquid in situ reaction. It was observed that the microstructure of the TiC_x/Al composites changed with changes in the reaction temperature and graphite particle size. With an increase in reaction temperature, the TiC_x particles in the TiC_x/Al composites transitioned from a spider-like distribution to being evenly dispersed in the Al matrix. Additionally, the morphology of the TiC_x particles changed from polygons of various sizes to quasi-spherical shapes with a uniform particle size, while the presence of Al_4C_3 and Al_3Ti in the matrix diminished. The size variation of the graphite particles had minimal impact on the particle size and stoichiometric ratio of TiC_x generated in the sample. Furthermore, an appropriate graphite particle size was found to mitigate the agglomeration and residue of graphite particles during the in situ reaction.

Keywords: particle-reinforced composites; Al-Ti alloy; TiC_x ; microstructure formation mechanism



Citation: Guo, L.; Sun, H.; Guo, Z. Synthesis of TiC_x/Al Composites via In Situ Reaction between Al_xTi Melt and Dissolvable Solid Carbon. *Metals* **2024**, *14*, 379. <https://doi.org/10.3390/met14040379>

Academic Editor: Georgios I. Giannopoulos

Received: 29 February 2024

Revised: 20 March 2024

Accepted: 22 March 2024

Published: 24 March 2024



Copyright: © 2024 by the authors. Licensee MDPI, Basel, Switzerland. This article is an open access article distributed under the terms and conditions of the Creative Commons Attribution (CC BY) license (<https://creativecommons.org/licenses/by/4.0/>).

1. Introduction

Aluminum-based composites (Al-based composites) are widely used to prepare lightweight equipment such as radiators, cylinder liners, and brake devices due to their high specific strength, specific elastic modulus, good wear resistance, and low thermal expansion coefficient [1–4]. High-performance Al-based composites can be obtained by introducing ceramic particles with high strength, good conductivity, and stability (such as carbides, oxides, borides, etc. [5–12]) into the Al matrix. Among them, TiC_x is widely used to prepare Al-based composites due to its high elastic modulus, high hardness, and high-temperature stability.

Currently, various methods for the preparation of TiC_x/Al composites have been developed (including discharge plasma sintering, mechanical mixing method, melt infiltration, powder metallurgy method, contact reaction method, etc. [13–18]). These methods are primarily categorized into ex situ and in situ methods, differing mainly in the introduction of the ceramic reinforcement phase. In the ex situ method, ceramic particles are directly added to the metal matrix from the outside, whereas in the in situ method, ceramic reinforcement phases are generated within the matrix directly through chemical reactions. Generally, the interface between the reinforcement phase and the metal matrix in composites synthesized by in situ methods is cleaner and straighter, and it exhibits a higher bonding strength compared to composites synthesized by ex situ methods [19,20]. In TiC_x/Al composites prepared through the in situ method, TiC_x forms a strong interface bond with the Al matrix, resulting in stronger mechanical properties and higher hardness than the matrix alloy. This method is crucial for the preparation of high-performance TiC_x/Al composites [21–23]. However, the traditional in situ method usually uses powdered raw materials to synthesize TiC_x/Al composites at a higher cost, which is generally more than four times that of bulk raw materials. At the same time, oxygen (O) easily forms an oxide layer on the surface of

titanium (Ti) powder, causing the oxide layer to dissolve into the matrix as a solid solute during the in situ preparation of TiC_x/Cu composites, reducing material performance.

The performance of in situ synthesized TiC_x/Al composites has been found to be mainly influenced by the stoichiometric ratio, distribution, and morphology of the TiC_x reinforcement phase, as well as the residual amount of harmful phases (Al_4C_3 and Al_3Ti) in the material [24–28]. Among these factors, the strengthening mechanism of TiC_x/Al composites is determined by the stoichiometric ratio, distribution, and morphology size of TiC_x , thereby affecting the physical and mechanical properties such as the flexural strength and wear resistance of the material. The performance of the material is improved when the TiC_x particle distribution in the TiC_x/Al composites is more uniform [29]. A large number of harmful phases (Al_4C_3 and Al_3Ti) are prepared in TiC_x/Al composite matrices using the traditional in situ method. The performance of the TiC_x/Al composites is affected by these two phases, damaging the interface between them and the matrix. Al_4C_3 is the product of the direct reaction between Al and C in the early stage of the in situ reaction of the Al-Ti-C system. It is easily decomposed into $\text{Al}(\text{OH})_3$ and CH_4 by a hydrolysis reaction with H_2O , resulting in interface damage between the Al_4C_3 and the matrix. This affects the transfer of stress between the Al_4C_3 and the matrix, thereby seriously damaging the stability of the composite properties [30]. The TiC_x/Al composite components undergo a slight deformation when exposed to moist air for a long time. Lu et al. [27] found that with the hydrolysis of Al_4C_3 in diamond/Al composites, the thermal conductivity and tensile strength of the material continued to decrease. Al_3Ti is a brittle phase and is easily broken under load, resulting in poor plasticity of TiC_x/Al composites. Yang et al. [28] found that reducing or eliminating the residual Al_3Ti phase in TiC_x/Al composites can further improve the tensile elongation and ultimate tensile strength of the composites. Therefore, the prerequisites for preparing high-performance and cost-effective TiC_x/Al composites include avoiding the residues of Al_4C_3 and Al_3Ti in TiC_x/Al composites, reducing preparation costs, and improving the distribution, stoichiometric ratio, and morphology of the TiC_x particles. Different reaction temperatures have a significant impact on the microstructure of TiC_x/Al composites, as found by Jiang et al. [31]. At higher reaction temperatures, the Al-Ti-C system further reacts and generates more TiC_x particles. Based on the above problems and the solid–liquid in situ reaction principle, in this study, there was very little Al_3Ti phase in the TiC_x/Al composites prepared by dissolving graphite particles from aluminum–titanium alloy, and no Al_4C_3 residue was found, which is useful for TiC_x/Al composites. The stability of the process has far-reaching consequences. At the same time, using bulk metal raw materials to prepare TiC_x/Al composites can avoid the defect of Ti powder easily introducing oxygen and greatly reduce the cost of raw materials. This opens up new ideas for producing TiC_x/Al composites with stable service performance and interface bonding strength.

In this paper, TiC_x/Al composites with different composition characteristics were successfully prepared by dissolving graphite particles from Al-Ti alloy. The influence of reaction temperature and holding time on the microstructure of the TiC_x/Al composites was revealed. The influence of different graphite particle raw materials on the morphology, particle size, volume fraction, and stoichiometry of TiC_x particles generated in the Al-Ti-C system was studied. The reaction sequence in the process of dissolving graphite particles from an Al-Ti alloy to prepare TiC_x/Al composites is further discussed. This is crucial to further optimize the performance of TiC_x/Al composites.

2. Materials and Methods

The raw materials used in the experiment were Al-10 wt%Ti alloy (99.99 wt% purity, 3–10 cm) and graphite particles (99.99 wt% purity, particle size 150–300, 100–150, 75–100, 60–75, and 46–60 μm). Scanning electron microscopy (SEM) images of Al-10 wt%Ti alloy and graphite particles of different particle sizes are shown in Figure 1.

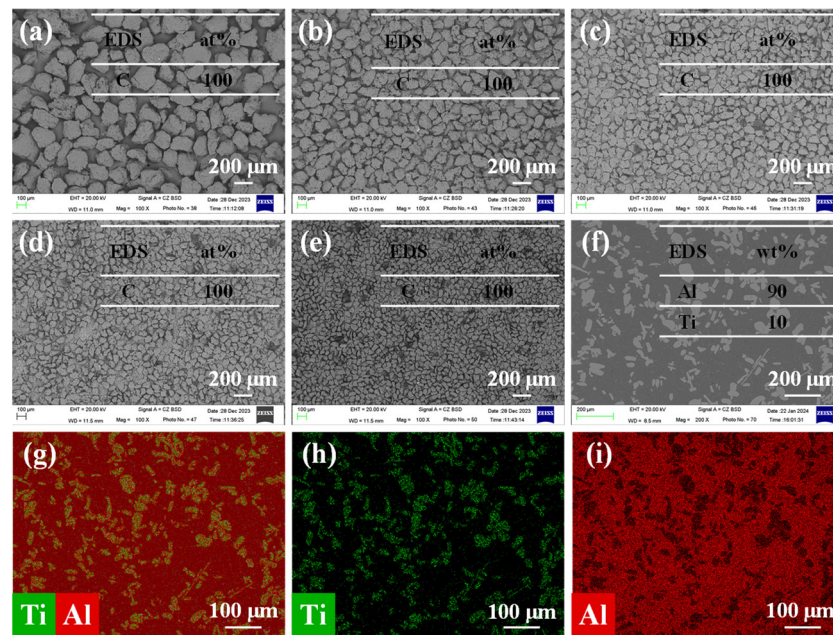


Figure 1. (a–e) SEM images of graphite particles with particle sizes of 150–300, 100–150, 75–100, 60–75, and 46–60 μm ; (f–i) SEM image and EDS surface of Al-10 wt%Ti alloy analysis.

In the process of preparing the TiC_x/Al composites, Al-Ti alloy and graphite particles (the molar ratio of C to Ti is 1:1) were mixed and placed in a porcelain boat, which was then placed in the constant-temperature zone of the horizontal tube furnace. Heating was performed under an argon atmosphere. The experimental groups and reaction conditions are shown in Table 1.

Table 1. Components and reaction conditions of TiC_x/Al composites in this study.

Sample No.	Sample Component	Graphite Particle Size (μm)	Temperature ($^{\circ}\text{C}$)	Holding Time (h)
A1	Al-10 wt%Ti + 2.5 wt%C	75–100 μm	1300 $^{\circ}\text{C}$	4 h
A2	Al-10 wt%Ti + 2.5 wt%C	75–100 μm	1400 $^{\circ}\text{C}$	4 h
A3	Al-10 wt%Ti + 2.5 wt%C	75–100 μm	1500 $^{\circ}\text{C}$	4 h
A4	Al-10 wt%Ti + 2.5 wt%C	75–100 μm	1600 $^{\circ}\text{C}$	4 h
B1	Al-10 wt%Ti + 2.5 wt%C	75–100 μm	1600 $^{\circ}\text{C}$	0.17 h
B2	Al-10 wt%Ti + 2.5 wt%C	75–100 μm	1600 $^{\circ}\text{C}$	1 h
B3	Al-10 wt%Ti + 2.5 wt%C	75–100 μm	1600 $^{\circ}\text{C}$	4 h
B4	Al-10 wt%Ti + 2.5 wt%C	75–100 μm	1600 $^{\circ}\text{C}$	8 h
C1	Al-10 wt%Ti + 2.5 wt%C	150–300 μm	1600 $^{\circ}\text{C}$	4 h
C2	Al-10 wt%Ti + 2.5 wt%C	100–150 μm	1600 $^{\circ}\text{C}$	4 h
C3	Al-10 wt%Ti + 2.5 wt%C	75–100 μm	1600 $^{\circ}\text{C}$	4 h
C4	Al-10 wt%Ti + 2.5 wt%C	60–75 μm	1600 $^{\circ}\text{C}$	4 h
C5	Al-10 wt%Ti + 2.5 wt%C	46–60 μm	1600 $^{\circ}\text{C}$	4 h

The prepared TiC_x/Al composites were cut, ground, and polished according to standard procedures. In order to avoid the hydrolysis of the Al_4C_3 phase during sample preparation, absolute ethanol was used to rinse the sample. The raw material composition, TiC_x/Al composites properties, and TiC_x stoichiometry were studied using SEM, energy dispersive spectrometer (EDS), and X-ray diffractometer (XRD, Rigaku-Smart Lab, Tokyo, Japan). The particle size distribution of TiC_x in the composite materials was obtained through Image-Pro Plus. In order to ensure the accuracy of the SEM-EDS detection of the raw material components, surface scans were performed in different areas, and the average value was taken.

3. Results

3.1. Raw Material Microstructure

As shown in Figure 1a–e, the graphite particles used in this study had an irregular block structure. The particle size statistical analysis revealed that the particle sizes ranged from 150–300, 100–150, 75–100, and 60–75 to 46–60 μm . The analysis of the Al-10 wt%Ti alloy revealed that Ti was uniformly distributed in the matrix in the form of Al_xTi compounds, as shown in Figure 1f–i.

3.2. Effect of Reaction Temperature and Reaction Time on TiC_x/Al Composites

The properties of the TiC_x/Al composites were significantly influenced by their phase composition, distribution, and morphology. The performance of the material was improved with a higher stoichiometric ratio and a more uniform distribution of TiC_x within the TiC_x/Al composites. Additionally, the stability of the material's performance was increased with a reduction of unstable phases within the TiC_x/Al composites. Phase formation in the TiC_x/Al composites was primarily influenced by the reaction temperature and reaction time. Therefore, the effect of reaction temperature and reaction time on the microstructure of TiC_x/Al composites is discussed in this section.

The study found that under the conditions of ensuring sufficient reaction time, the microstructure of the TiC_x/Al composites generated by the Al-10Ti-2.5C system at different reaction temperatures changed significantly. Figure 2 shows the XRD images of TiC_x/Al composites prepared at different reaction temperatures. All samples contained TiC_x , which shows that the Al-Ti melt and graphite particles can react with carbon–titanium to synthesize TiC_x .

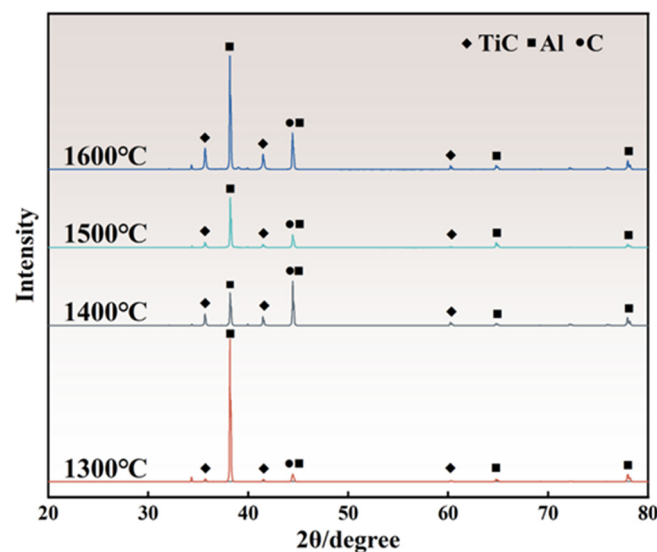


Figure 2. XRD of TiC_x/Al composites prepared at different reaction temperatures.

To further analyze the distribution and morphology of TiC_x , the SEM image of the sample was partitioned into three regions: upper, middle, and lower, as shown in Figure 3. The investigation revealed that the TiC_x in the samples synthesized at lower reaction temperatures exhibited a network-like distribution. As the reaction temperature increased (e.g., 1500 °C and 1600 °C), the TiC_x generated in the samples showed a more uniform distribution. This indicates that the TiC_x formed at lower reaction temperatures was primarily distributed along the grain boundaries of the Al grains, while at higher reaction temperatures, the TiC_x was evenly dispersed within the Al matrix.

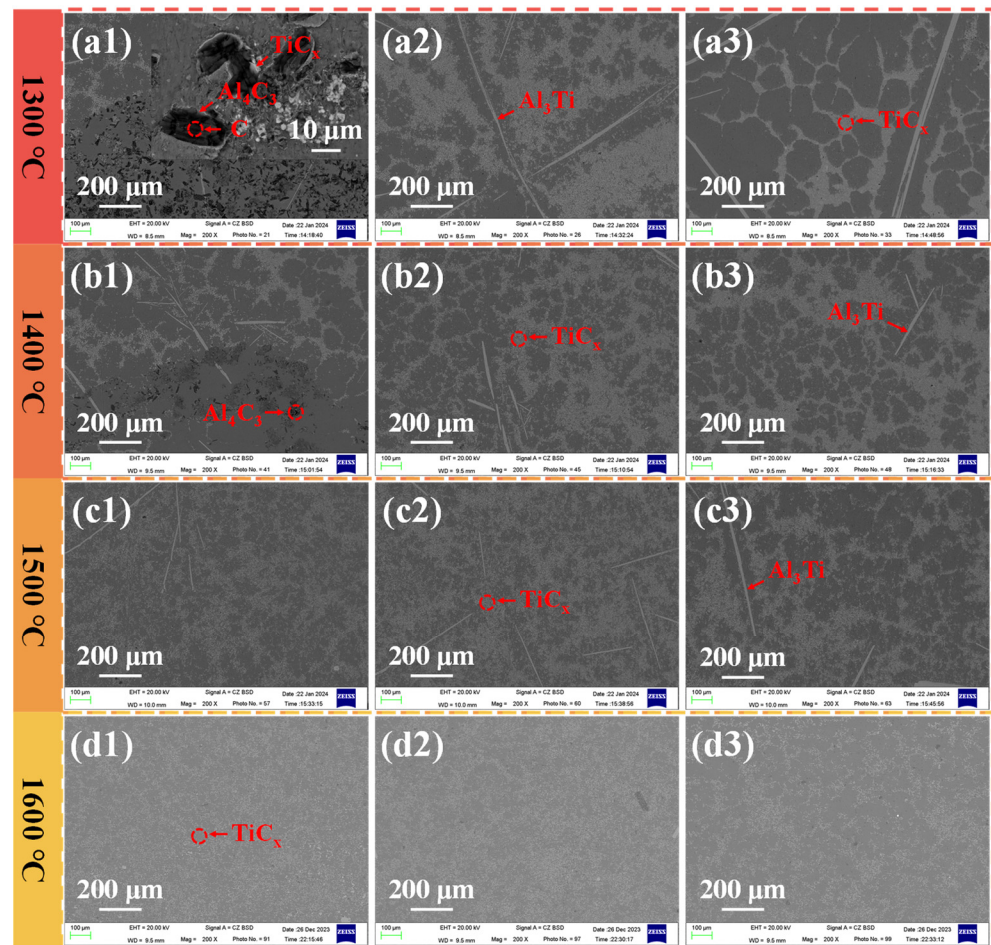


Figure 3. SEM images of TiC_x/Al composites produced at different reaction temperatures: (a1–a3) A1 sample; (b1–b3) A2 sample; (c1–c3) A3 sample; (d1–d3) A4 sample.

When the reaction temperature of the Al-10Ti-2.5C system was low, a large amount of Al_4C_3 and Al_3Ti phases were found in the sample, which affected the stability and plasticity of the TiC_x/Al composites during service. A three-layer core–shell structure ($\text{C}@ \text{Al}_4\text{C}_3 @ \text{TiC}_x$) was observed in the TiC_x/Al composites prepared by the Al-10Ti-2.5C system at 1300 °C and 1400 °C, composed of incompletely reacted graphite, Al_4C_3 , and TiC_x , as shown in Figure 3(a1–b3). However, similar core–shell structures were not observed in the samples prepared at 1500 °C and 1600 °C, as shown in Figure 3(c1–d3). It was demonstrated that the Al_4C_3 generated by the reaction between graphite particles and high-temperature Al-Ti melt reacted with Ti in the Al-Ti melt at the $\text{Al}_4\text{C}_3/\text{melt}$ interface to form TiC_x and completely react at a higher temperature. This was because the fluidity of the melt was improved by increasing the reaction temperature, and the activity of the reactants was increased. As the reaction temperature was increased, the residual Al_3Ti in the TiC_x/Al composites gradually decreased. Changes in the microstructure of the TiC_x/Al composites were affected by keeping the reaction temperature of the Al-10Ti-2.5C system unchanged and extending or reducing the reaction time, as depicted in Figure 4. There was no residual Al_4C_3 in the samples of group B, indicating that Al_4C_3 rapidly reacted with Ti in the melt to form TiC_x at 1600 °C. With the prolongation of the reaction time, the long Al_3Ti phase in the melt broke down and further reacted with the C dissolved into the matrix to form TiC_x or promote the increase in the stoichiometric ratio of TiC_x . With the further reaction of the Al_3Ti phase, the volume fraction of TiC_x in the TiC_x/Al composites also significantly increased.

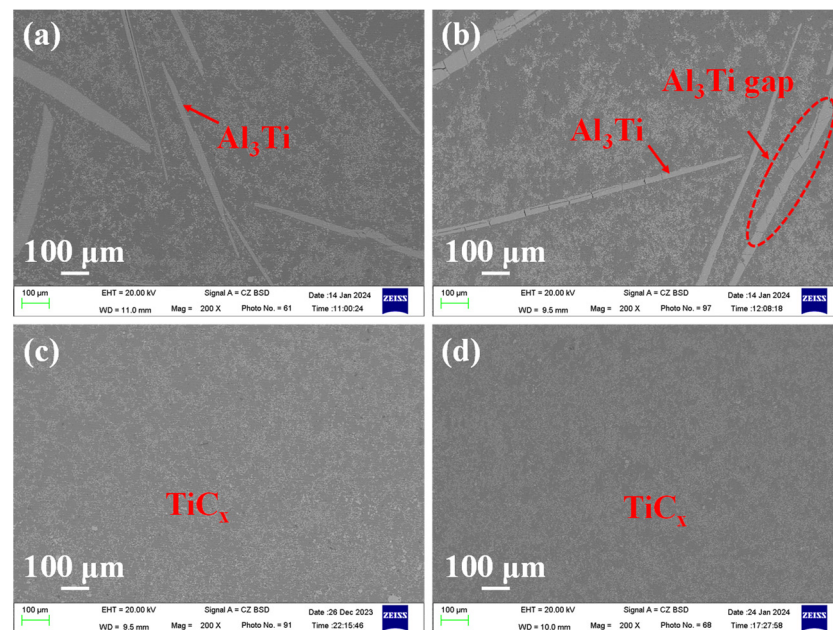


Figure 4. SEM images of TiC_x/Al composites produced under different reaction times: (a) B1 sample; (b) B2 sample; (c) B3 sample; (d) B4 sample.

The characteristics of no Al_4C_3 phase residue, very little Al_3Ti phase distribution, and uniformly distributed TiC_x particles were observed in the TiC_x/Al composites prepared by the Al-10Ti-2.5C system at 1600 °C and maintained for a long time, as shown in this study, and improvements in the material properties and performance stability during service are facilitated by these characteristics.

As depicted in Figure 5, it was found through EDS analysis that the TiC_x generated in the Al-10Ti-2.5C system contained a small amount of Al, with the C content slightly higher than Ti. With increasing reaction temperature, the proportion of Al atoms in the TiC_x generated in the sample gradually decreased. This phenomenon arose because the TiC_x in the sample was primarily formed through the reaction of Al_4C_3 and Ti rather than the direct reaction of graphite and Ti. By observing the morphology and particle size of the TiC_x in samples prepared at different temperatures, it was found that as the reaction temperature increased, the morphology of TiC_x changed from irregular polygonal to nearly spherical, with the particle size further increases. Jin et al. [32] indicate that during the growth process of TiC_x , the stoichiometric ratio approaches 1, and the shape tends to be spherical. This indicates that the rise in reaction temperature of the Al-10Ti-2.5C system also contributes to an increase in the TiC_x stoichiometric ratio. As shown in Figure 6e–h, as the reaction time is extended, the proportion of Al atoms in TiC_x gradually diminishes while the proportions of Ti and C atoms stabilize. However, a further extension of the reaction time in the Al-10Ti-2.5C system does not significantly increase the proportion of Ti atoms in TiC_x . This is because the concentration of Ti atoms in the melt continues to decrease, leading to a gradual slowing of the growth rate of TiC_x , eventually approaching 0. This study found that with the increase in the reaction temperature and holding time, the disappearance of Al_4C_3 , the decrease in Al_3Ti in the TiC_x/Al composites, and the increase in the dispersion of the TiC_x volume fraction further promoted a reduction in the matrix grain size and increased the effect of fine grain strengthening, improving the hardness and other mechanical properties of the material.

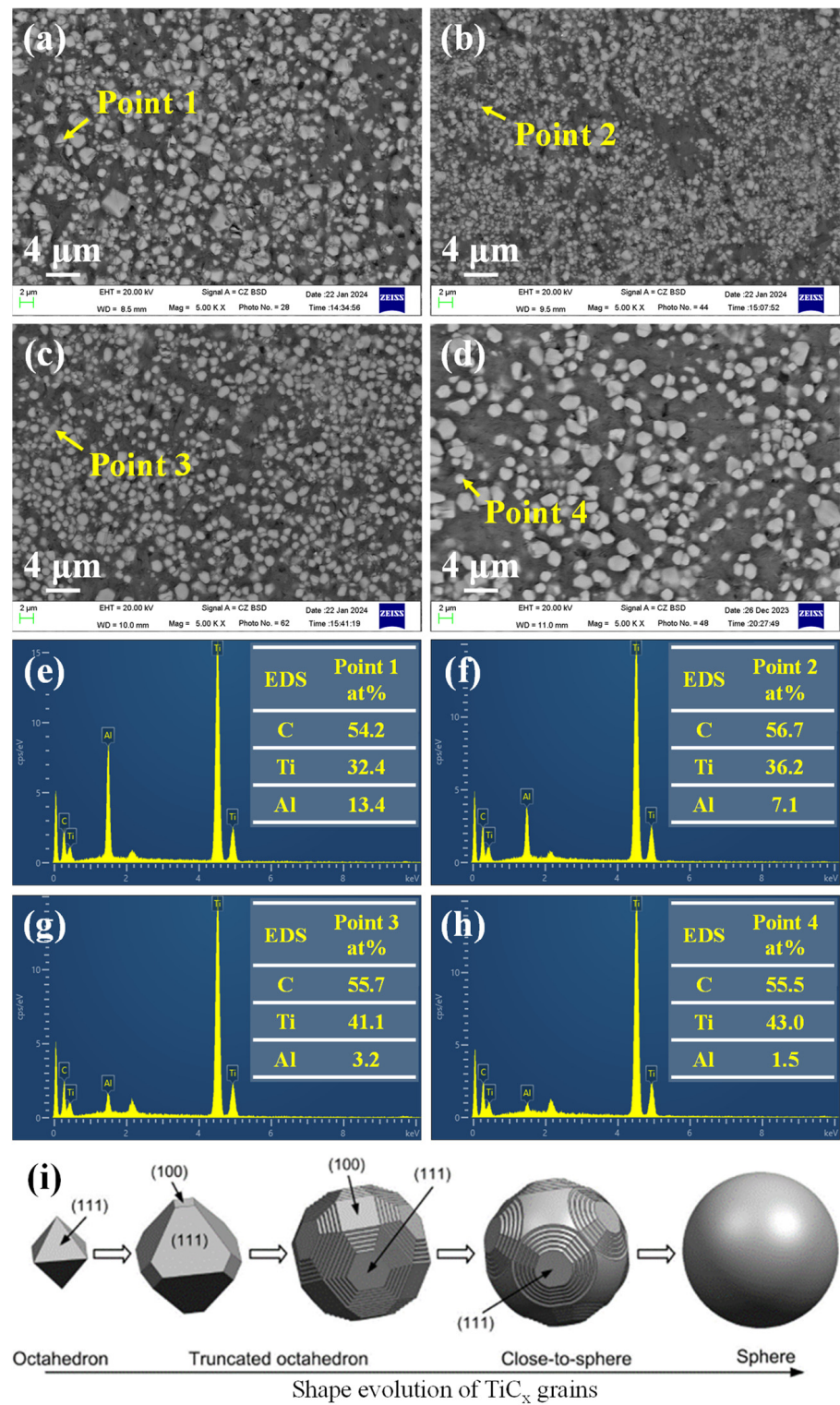


Figure 5. (a) A1 sample; (b) A2 sample; (c) A3 sample; (d) A4 sample; (e–h) EDS analysis results corresponding to Point1–Point4; (i) the relationship between stoichiometric ratio and morphology during the TiC_x generation process [32].

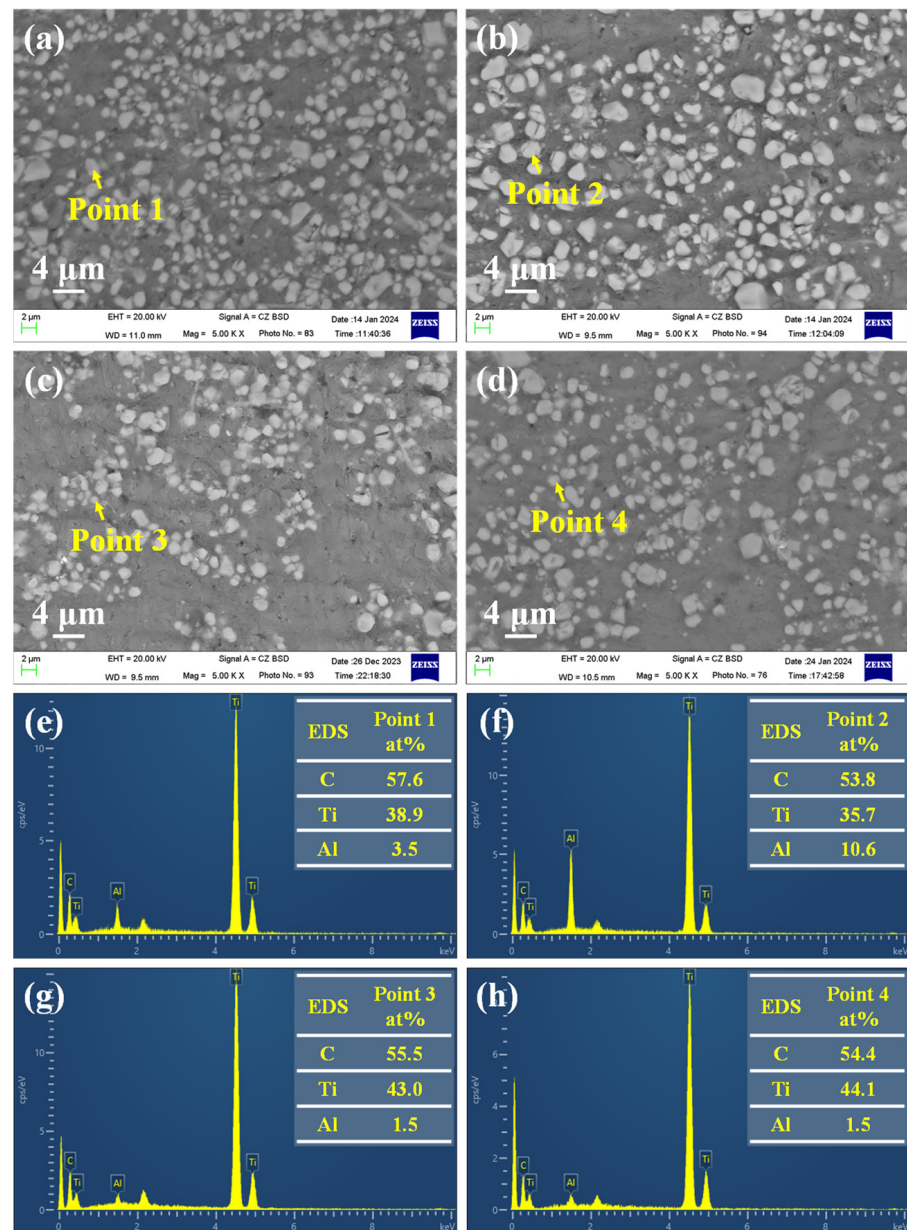


Figure 6. SEM images and EDS analysis of TiC_x in TiC_x/Al composites produced under different reaction times: (a,e) B1 sample; (b,f) B2 sample; (c,g) B3 sample; (d,h) B4 sample.

3.3. Effect of Graphite Particle Size on TiC_x/Al Composites

The particle size variation of the TiC_x reinforcement phase in TiC_x/Al composites significantly affects the material's properties. The smaller particle size of TiC_x particles corresponds to the enhanced performance of TiC_x/Al composites. The particle size of the graphite particle raw material plays a crucial role in determining the particle size of TiC_x generated in the Al-10Ti-2.5C system. Hence, this section explores the influence of different graphite particle sizes on the TiC_x particle size in TiC_x/Al composites.

When the particle size of the graphite particle raw material is smaller than a specific value, the graphite particles will directly react with Ti in the Al-Ti melt to generate TiC_x . However, during the solid-liquid in situ reaction, graphite particles that are too small are prone to agglomeration, causing the graphite particles to be unable to be completely wetted by the Al-Ti melt, thus leaving unreacted graphite particles in the sample. At the same time, excessively large graphite particles will remain due to the decreasing activity of Ti atoms in the Al-Ti melt. This section uses graphite particles of different particle sizes

as carbon sources to study the effect of graphite particle size on the microstructure of TiC_x/Al composites prepared by this method. As shown in Figure 7, the phenomena when graphite particles of different sizes react with Al-Ti alloy melt are basically the same. In order to analyze the differences in the microstructure of group C samples further, each TiC_x -containing region was divided into upper, middle, and lower parts. As shown in Figure 7, the TiC_x generated in the sample gradually becomes further dispersed as the graphite particle size decreases.

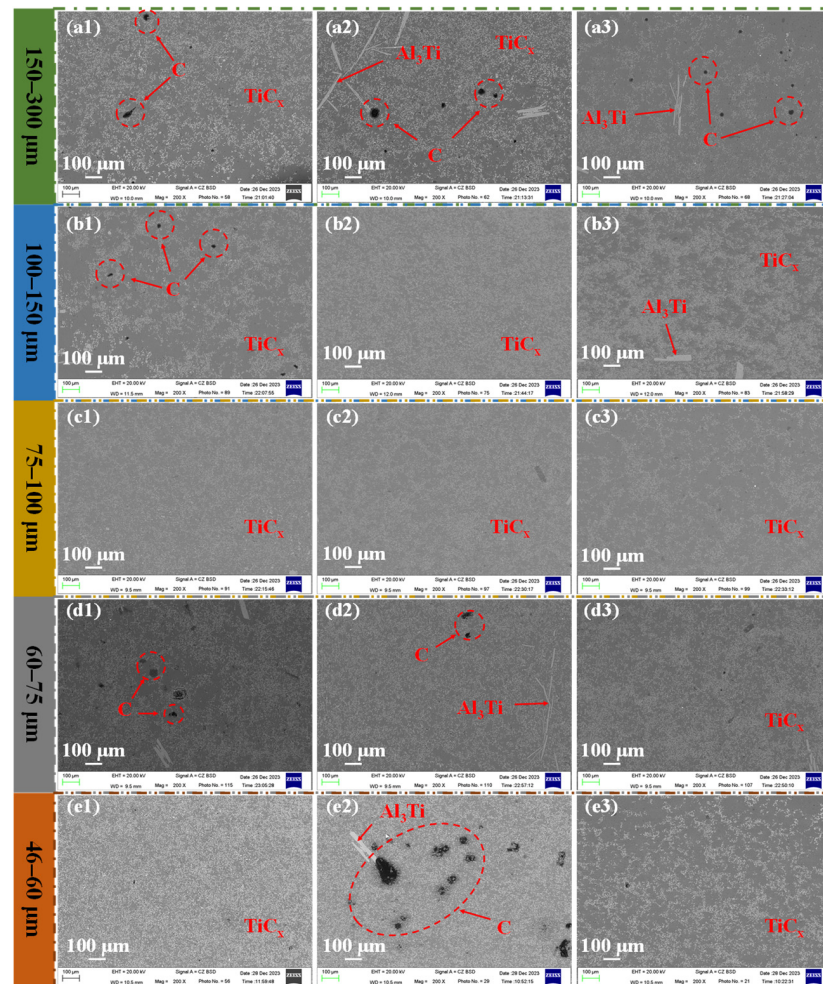


Figure 7. SEM image of the TiC_x/Al composites: (a1–a3) C1 sample; (b1–b3) C2 sample; (c1–c3) C3 sample; (d1–d3) C4 sample; (e1–e3) C5 sample.

As shown in Figure 7(c1–e3), when the graphite particle size is $<100 \mu m$, the distribution of each region in the TiC_x sample is basically the same, and as the graphite particle size further decreases, the degree of dispersion of TiC_x in different samples remains unchanged. When the particle size of graphite particles is $>100 \mu m$, the degree of TiC_x dispersion in different areas of the sample varies greatly. When the graphite particle size is between 150–300 and 100–150 μm , there are more unreacted graphite particles and Al_3Ti remaining in the sample matrix, as shown in Figure 7(a1–b3). When the graphite particle sizes are 60–75 and 46–60 μm , a small amount of agglomerated graphite particles and unreacted Al_3Ti phase remain in the sample, as shown in Figure 7(d1–e3). As shown in Figure 8, different graphite raw material particle sizes have little effect on the stoichiometry of TiC_x in the prepared composite materials. As shown in Figure 9, the particle size of TiC_x generated by the reaction in different samples is basically around 2 μm , and the TiC_x with particle size $<3 \mu m$ in the sample accounts for more than 86%. The study found that when the graphite particle size was 75–100 μm , the sample's TiC_x with particle size $<3 \mu m$ was at

most 98.9%. Therefore, when the Al-10 wt%Ti alloy reacted with graphite particles with a particle size of 75–100 μm at 1600 $^{\circ}\text{C}$, the TiC_x in the generated TiC_x/Al composites was the most uniform, the average particle size was the smallest, and the residual amounts of Al_4C_3 and Al_3Ti phases in the matrix are the lowest.

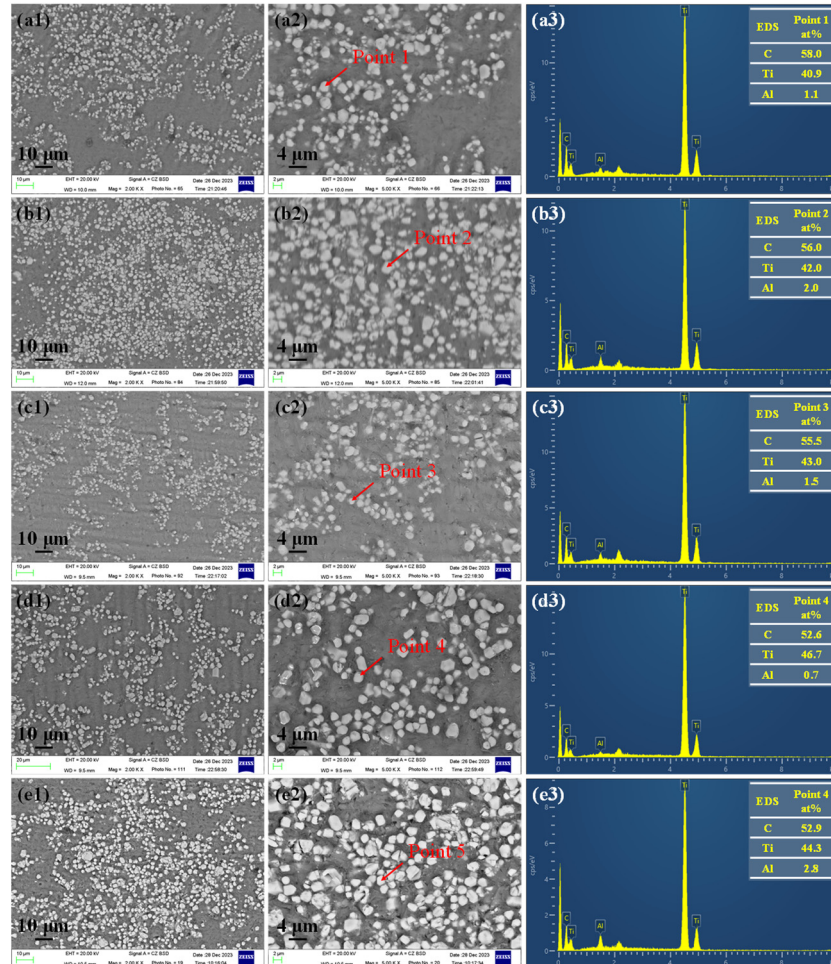


Figure 8. SEM images and EDS analysis of TiC_x in different TiC_x/Al composites: (a1–a3) C1 sample; (b1–b3) C2 sample; (c1–c3) C3 sample; (d1–d3) C4 sample; (e1–e3) C5 sample.

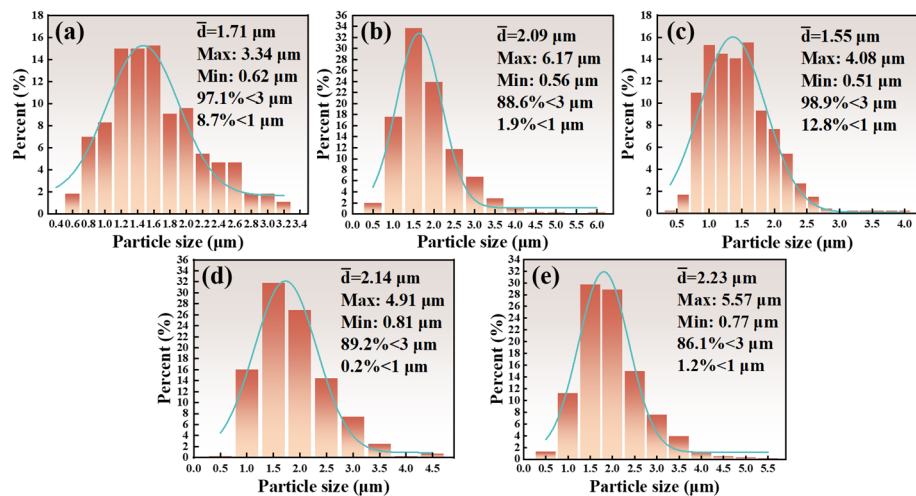


Figure 9. Particle size analysis of TiC_x in different TiC_x/Al composites: (a) C1 sample; (b) C2 sample; (c) C3 sample; (d) C4 sample; (e) C5 sample.

3.4. Synthesis Sequence of TiC_x in Al-10Ti-2.5C System

According to current research findings, when Al-Ti melt dissolves graphite particles in situ to synthesize TiC_x /Al composites, the following reactions may occur:



In previous studies, we also tried to use Al-Ti melt to dissolve graphite particles to prepare TiC_x /Al composites at a lower reaction temperature (higher than the melting point of Al-Ti alloy). However, studies have found that too low a reaction temperature will result in poor fluidity of the Al-Ti melt and the inability to completely wet the graphite particles, resulting in the incomplete reaction of the graphite particles. By comparison, it was found that increasing the reaction temperature can improve the fluidity of the Al-Ti melt, better wet the graphite particles, and generate a large amount of TiC_x reinforcement phase.

Analyzing the microstructure of TiC_x /Al composites prepared under different conditions revealed the synthesis sequence of TiC_x in the Al-10Ti-2.5C system, as depicted in Figure 10. When the high-temperature Al-Ti melt contacts graphite particles, Al reacts rapidly with the graphite particles on the surface of the graphite particles to generate a large amount of Al_4C_3 , and some graphite particles dissolve into Al in the form of C atoms (Figure 10a,b). As the reaction proceeds, the smaller graphite particles are completely transformed into Al_4C_3 particles, while a continuous Al_4C_3 layer is formed on the surface of the larger graphite particles (Figure 10c). In Al-Ti alloys, Ti primarily exists in the form of Al_3Ti . Upon melting, Al_3Ti readily forms a molten Al-Ti layer within the Al melt, causing the dispersion of Ti in the Al-Ti melt (Figure 10b) [33]. At this stage, Ti dispersed in the melt reacts with C at the Al_4C_3 /melt interface to generate TiC_x , while the solid C solution in Al reacts with Ti near the Al-Ti layer to produce TiC_x (Figure 10c). As the thickness of the TiC_x layer in the Al_4C_3 surface continues to increase, cracks gradually manifest in the TiC_x layer, dispersing into smaller TiC_x particles within the melt (Figure 10d,e). Concurrently, the surface of Al_4C_3 forms a new TiC_x layer as the previous TiC_x layer fractures. This cycle of changes in Al_4C_3 within the Al-Ti melt persists until all of the Al_4C_3 is converted into TiC_x . As the thickness of the TiC_x layer in the Al_4C_3 surface continues to increase, cracks gradually manifest in the TiC_x layer, dispersing into smaller TiC_x particles within the melt (Figure 10d–f). Simultaneously, with the extension of the reaction time and the continuous depletion of Ti, the long strips of Al_3Ti gradually break into short rods and are gradually consumed completely (Figure 10d–f). However, due to the ongoing reduction in the Ti concentration within the Al-Ti melt, the rate of the carbon–titanium reaction gradually diminishes, approaching 0, leading to the presence of individual small-sized Al_3Ti phases remaining in the matrix.

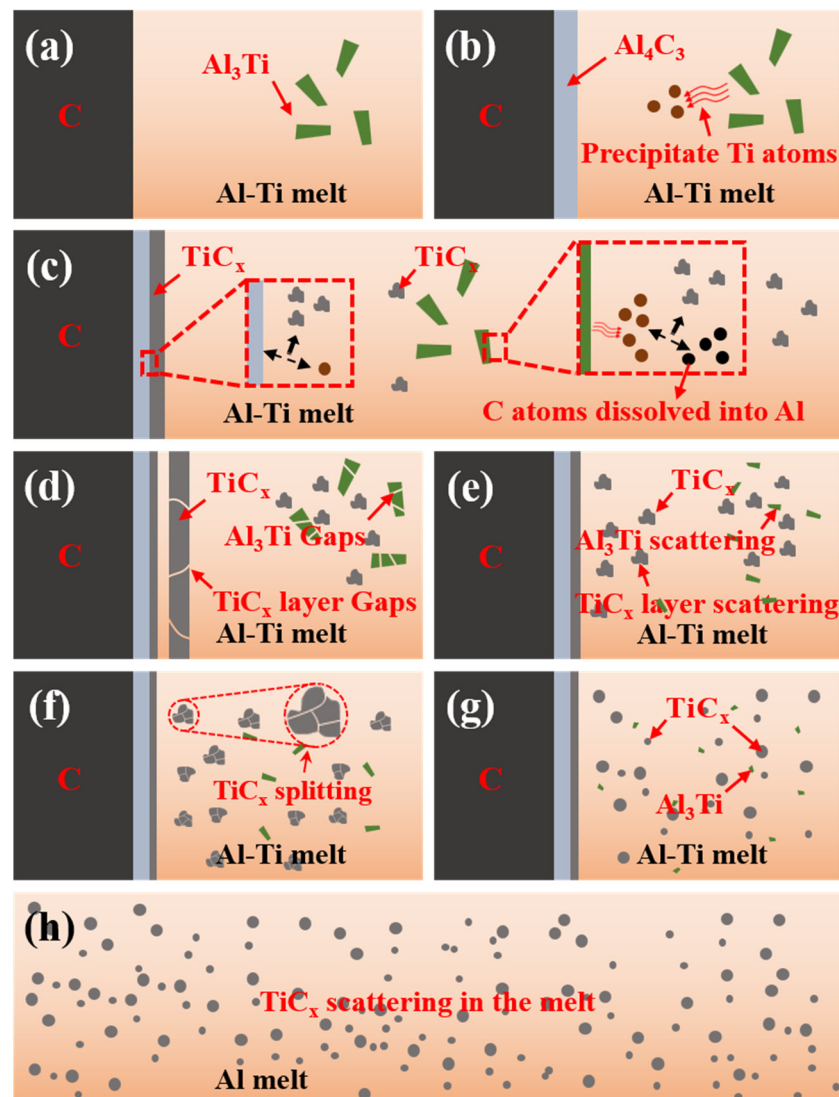


Figure 10. (a–h) The processes from when the graphite particles are in contact with the aluminum–titanium melt to when the graphite particles are completely reacted are shown, respectively.

4. Conclusions

In this study, TiC_x/Al composites were successfully fabricated by dissolving graphite particles in an Al-Ti melt. The experimental results indicate that the TiC_x reinforcement phase in these composites tends to distribute evenly throughout the matrix, with the microstructure of TiC_x and residual phases changing in response to changes in reaction temperature and initial graphite particle size. The investigation reveals that as the reaction temperature increases, the TiC_x particles in the TiC_x/Al composites produced via the Al-Ti melt dissolution of graphite particles exhibit a more uniform distribution, and their morphology gradually transitions toward a spherical shape. In addition, the Ti-C reaction is easily affected by the Al-C reaction at lower reaction temperatures, resulting in the presence of the Al_4C_3 phase and unreacted Al_3Ti phase in the sample. Interestingly, different graphite particle sizes have minimal impact on the stoichiometric ratio, morphology, and volume fraction of the generated TiC_x . Larger graphite particles persist due to decreased Ti activity in the melt. Conversely, excessively small graphite particles tend to agglomerate in the Al-Ti melt, hindering complete wetting by the melt and remaining within the matrix.

Author Contributions: Conceptualization, L.G. and Z.G.; Funding acquisition, L.G. and Z.G.; Supervision, L.G. and Z.G.; Writing—Review and Editing, L.G. and Z.G.; Writing—Original Draft, H.S.; Experimentation, H.S.; Design, H.S.; Data management, H.S.; Verification, H.S.; Project administration, Z.G. All authors have read and agreed to the published version of the manuscript.

Funding: This work was supported by the National Key R&D Program Project 2022YF-C2906100, the National Natural Science Foundation of China (No.51804030 and 52174275).

Data Availability Statement: The raw data supporting the conclusions of this article will be made available by the authors on request.

Conflicts of Interest: The authors declare no conflicts of interest.

References

1. Korkut, M.H. Effect of particulate reinforcement on wear behaviour of aluminium matrix composites. *Mater. Sci. Technol.* **2004**, *20*, 73–81. [[CrossRef](#)]
2. Suárez, O.M. Mechanical Properties of a Novel Aluminum Matrix Composite Containing Boron. *J. Mech. Behav. Mater.* **2001**, *12*, 225–238. [[CrossRef](#)]
3. Martínez, M.A.; Martín, A.; Llorca, J. Wear of Al-Si alloys and Al-Si/SiC composites at ambient and elevated temperatures. *Scr. Metall. Mater.* **1993**, *28*, 207–212. [[CrossRef](#)]
4. Yin, Z.J.; Tao, S.Y.; Zhou, X.M.; Ding, C.X. Microstructure and mechanical properties of Al₂O₃-Al composite coatings deposited by plasma spraying. *Appl. Surf. Sci.* **2008**, *254*, 1636–1643. [[CrossRef](#)]
5. Song, M. Effects of volume fraction of SiC particles on mechanical properties of SiC/Al composites. *Trans. Nonferrous Met. Soc. China* **2009**, *19*, 1400–1404. [[CrossRef](#)]
6. Dong, Y.; Chen, A.; Yang, T.; Gao, S.; Liu, S.N.; Guo, B.J.; Jiang, H.Y.; Shi, Y.S.; Yan, C.Z. Microstructure evolution and mechanical properties of Al₂O₃ foams via laser powder bed fusion from Al particles. *Adv. Powder Mater.* **2023**, *2*, 100135. [[CrossRef](#)]
7. Xu, J.; Li, Z.Y.; Zhu, W.H.; Liu, Z.L.; Liu, W.J. Investigation on microstructural characterization of in situ TiB/Al metal matrix composite by laser cladding. *Mater. Sci. Eng. A* **2007**, *447*, 307–313. [[CrossRef](#)]
8. Pourkhorshid, E.; Enayati, M.H.; Sabooni, S.; Karimzadeh, F.; Paydar, M.H. Bulk Al-Al₃Zr composite prepared by mechanical alloying and hot extrusion for high-temperature applications. *Int. J. Miner. Metall. Mater.* **2017**, *24*, 937–942. [[CrossRef](#)]
9. Ding, H.M.; Wu, J.M.; Jia, H.R.; Liu, F.; Wang, J.F. The Influence of Carbon Sources on the Microstructures of In Situ-Synthesized TiC in Al Melts. *Materials* **2022**, *15*, 4610. [[CrossRef](#)]
10. Lee, J.C.; Lee, H.I.; Ahn, J.P.; Shi, Z.L.; Kim, Y.M. Modification of the interface in SiC/Al composites. *Metall. Mater. Trans. A* **2000**, *31*, 2361–2368. [[CrossRef](#)]
11. Yang, H.Y.; Wang, Z.; Chen, L.Y.; Shu, S.L.; Qiu, F.; Zhang, L.C. Interface formation and bonding control in high-volume-fraction (TiC+ TiB₂)/Al composites and their roles in enhancing properties. *Compos. Part B Eng.* **2021**, *209*, 108605. [[CrossRef](#)]
12. Jiang, R.S.; Chen, X.F.; Ge, R.W.; Wang, W.H.; Song, G.D. Influence of TiB₂ particles on machinability and machining parameter optimization of TiB₂/Al MMCs. *Chin. J. Aeronaut.* **2018**, *31*, 187–196. [[CrossRef](#)]
13. Sattariand, S.; Atrian, A. Effects of the deep rolling process on the surface roughness and properties of an Al-3vol%SiC nanoparticle nanocomposite fabricated by mechanical milling and hot extrusion. *Int. J. Miner. Metall. Mater.* **2017**, *24*, 814–825. [[CrossRef](#)]
14. Wang, F.; Li, Y.P.; Wang, X.; Koizumi, Y.; Kenta, Y.; Chiba, A. In-situ fabrication and characterization of ultrafine structured Cu-TiC composites with high strength and high conductivity by mechanical milling. *J. Alloys Compd.* **2016**, *657*, 122–132. [[CrossRef](#)]
15. Khorrami, M.S.; Kazeminezhad, M.; Miyashita, Y.; Kokabi, A.H. Improvement in the mechanical properties of Al/SiC nanocomposites fabricated by severe plastic deformation and friction stir processing. *Int. J. Miner. Metall. Mater.* **2017**, *24*, 297–308. [[CrossRef](#)]
16. Chak, V.; Chattopadhyay, H.; Dora, T.L. A review on fabrication methods, reinforcements and mechanical properties of aluminum matrix composites. *J. Manuf. Process.* **2020**, *56*, 1059–1074. [[CrossRef](#)]
17. Hu, Z.J.; Shen, P.; Jiang, Q.C. Developing high-performance laminated Cu/TiC composites through melt infiltration of Ni-doped freeze-cast preforms. *Ceram. Int.* **2019**, *45*, 11686–11693. [[CrossRef](#)]
18. Amosov, A.; Amosov, E.; Latukhin, E.; Kichaev, P.; Umerov, P. Producing TiC-Al Cermet by Combustion Synthesis of TiC Porous Skeleton with Spontaneous Infiltration by Aluminum Melt. In Proceedings of the 2020 7th International Congress on Energy Fluxes and Radiation Effects (EFRE), Tomsk, Russia, 14–26 September 2020.
19. Huang, X.; Bao, L.K.; Bao, R.; Liu, L.; Tao, J.M.; Wang, J.S.; Zhang, Z.F.; Ge, Z.H.; Tan, S.L.; Yi, J.H.; et al. Reinforced copper matrix composites with highly dispersed nano size TiC in-situ generated from the Carbon Polymer Dots. *Adv. Powder Mater.* **2023**, *2*, 2772–2834X. [[CrossRef](#)]
20. Li, W.J.; Zhang, L.; Chen, Z.Y.; Shao, W.Z.; Zhen, L. In Situ Fabrication and Static Contact Resistance of CdMoO₄ Reinforced Cu Matrix Composites. *Materials* **2022**, *15*, 7206. [[CrossRef](#)] [[PubMed](#)]
21. Jin, S.B.; Shen, P.; Zhou, D.S.; Jiang, Q.C. Self-propagating high-temperature synthesis of nano-TiC_x particles with different shapes by using carbon nano-tube as C source. *Nanoscale Res. Lett.* **2011**, *6*, 515. [[CrossRef](#)] [[PubMed](#)]

22. Yang, Y.F.; Mu, D.K. Rapid dehydrogenation of TiH_2 and its effect on formation mechanism of TiC during self-propagation high-temperature synthesis from TiH_2 -C system. *Powder Technol.* **2013**, *249*, 208–211. [[CrossRef](#)]
23. Song, M.S.; Zhang, M.X.; Zhang, S.G.; Huang, B.; Li, J.G. In situ fabrication of TiC particulates locally reinforced aluminum matrix composites by self-propagating reaction during casting. *Mater. Sci. Eng. A* **2008**, *473*, 166–171. [[CrossRef](#)]
24. Wang, L.; Qiu, F.; Zhao, Q.L.; Zha, M.; Jiang, Q.C. Superior high creep resistance of in situ nano-sized TiC_x /Al-Cu-Mg composite. *Sci. Rep.* **2017**, *7*, 4540. [[CrossRef](#)]
25. Tian, W.S.; Zhao, Q.L.; Zhang, Q.Q.; Qiu, F.; Jiang, Q.C. Superior creep resistance of 0.3 wt% nano-sized TiC_p /Al-Cu composite. *Mater. Sci. Eng. A* **2017**, *700*, 42–48. [[CrossRef](#)]
26. Zhou, D.S.; Qiu, F.; Jiang, Q.C. The nano-sized TiC particle reinforced Al-Cu matrix composite with superior tensile ductility. *Mater. Sci. Eng. A* **2015**, *622*, 189–193. [[CrossRef](#)]
27. Lu, Y.; Wang, X.; Zhang, Y.; Wang, J.; Kim, M.J.; Zhang, H. Aluminum carbide hydrolysis induced degradation of thermal conductivity and tensile strength in diamond/aluminum composite. *J. Compos. Mater.* **2018**, *52*, 2709–2717. [[CrossRef](#)]
28. Yang, B.; Chen, G.X.; Zhang, J.S. Effect of Ti/C additions on the formation of Al_3Ti of in situ TiC/Al composites. *Mater. Des.* **2001**, *22*, 645–650. [[CrossRef](#)]
29. Tian, W.S.; Zhao, Q.L.; Zhao, C.J.; Qiu, F.; Jiang, Q.C. The Dry Sliding Wear Properties of Nano-Sized TiC_p /Al-Cu Composites at Elevated Temperatures. *Materials* **2017**, *10*, 939. [[CrossRef](#)] [[PubMed](#)]
30. Cao, J.M.; Li, F.J.; Yang, Q.C.; Zhan, K.; Yang, Z.; Wang, Z.; Zhao, B. A review on interfacial structure optimization and its mechanism on the properties of carbon reinforced metal-matrix composites. *Compos. Interfaces* **2023**, *30*, 543–583. [[CrossRef](#)]
31. Jiang, W.H.; Song, G.H.; Han, X.L.; He, C.L.; Ru, H.C. Synthesis of TiC/Al composites in liquid aluminium. *Mater. Lett.* **1997**, *32*, 63–65. [[CrossRef](#)]
32. Jin, S.B.; Shen, P.; Lin, Q.L.; Zhan, L.; Jiang, Q.C. Growth Mechanism of TiC_x during Self-Propagating High-Temperature Synthesis in an Al-Ti-C System. *Cryst. Growth Des.* **2010**, *10*, 1590–1597. [[CrossRef](#)]
33. Chen, T.J.; Wang, R.Q.; Ma, Y.; Hao, Y. Grain refinement of AZ91D magnesium alloy by Al-Ti-B master alloy and its effect on mechanical properties. *Mater. Des.* **2012**, *34*, 637–648. [[CrossRef](#)]

Disclaimer/Publisher’s Note: The statements, opinions and data contained in all publications are solely those of the individual author(s) and contributor(s) and not of MDPI and/or the editor(s). MDPI and/or the editor(s) disclaim responsibility for any injury to people or property resulting from any ideas, methods, instructions or products referred to in the content.